Computer simulation of Feynman's ratchet and pawl system

Jianzhou Zheng, Xiao Zheng, ChiYung Yam, and GuanHua Chen*
Department of Chemistry, University of Hong Kong, Hong Kong, China
(Received 16 December 2009; revised manuscript received 28 February 2010; published 2 June 2010)

In this work, we introduce two models of Feynman's ratchet and pawl system. Molecular dynamics is carried out to simulate the two designs for Feynman's ratchet and pawl systems followed by a Langevin dynamics simulation of the reduced system. We find that the ratchet will rotate as designed when the temperature of the pawl chamber is lower than that of the ratchet chamber, which is consistent with the second law of thermodynamics. Different parameters and configurations are tested, and the results show that the efficiency of the ratchet depends on the applied torque. We find further that efficiencies of the Feynman's ratchet and pawl systems depend greatly on the details of the systems.

DOI: 10.1103/PhysRevE.81.061104 PACS number(s): 05.70.−a, 45.20.D−

I. INTRODUCTION

Maxwell's demon was introduced by Maxwell in 1871 [1,2]. In his setting, there are two chambers filled with moving gas particles and separated by a wall with a hole in the center. Maxwell's demon is an intelligent being sitting beside the hole. It allows only hot particles go to the left chamber and cool particles go to the right chamber. After some time, most of the hot particles will go to the left chamber and the cool particles will go to the right chamber. As a result, there will be a temperature difference between the two chambers.

According to the second law of thermodynamics, there should not be such a demon that reduces continuously the entropy of the entire isolated system. On the other hand, when a system is out of equilibrium, a demon of this kind may work under special conditions.

There have been many debates on the existence of such a demon and its functionality. Recently, with the developments of nanotechnologies, the prospects of testing fundamental hypotheses of thermodynamics and realizing Maxwell's demons at nanoscale have been contemplated [3–9].

Smoluchowski, in his paper [10], pointed out that thermal fluctuations would prevent any automatic device from operating successfully as a Maxwell's demon in 1912. Up to now, most of investigations on Maxwell's demon have been thought experiments. Lasting interests in Maxwell's demon and incessant quests have been documented in the literature. However, only a few microscopic simulations have been carried out to examine the detailed behavior of Maxwell's demons. Zhang and Zhang [11] formulated a set of sufficient conditions for the survival of a Maxwell's demon. In 1992, a trap-door device was studied for the first time via numerical simulation by Skordos and Zurek [12]. Their results show that the trap door can act as a pump and cannot extract useful work from the thermal motion of hot molecules. Leff and Rex [13] later searched the different configurations of the trap door, and found an optimal configuration for which the net entropy change is zero.

In 1963, Feynman *et al.* introduced a ratchet and pawl system [14]. The system is consisted of two chambers. In one chamber, a ratchet can rotate easily in one direction but will be hindered by an asymmetric pawl in the other direction. The ratchet is immersed in a bath of molecules with temperature T_1. In the other chamber, there is a paddle wheel which is immersed in another bath with temperature T_2. The ratchet and the paddle wheel are rigidly connected by frictionless rod with zero mass. In this setting, both the ratchet and the paddle undergo Brownian motions with mean kinetic energies which are determined by the temperatures of the related baths. After colliding between the molecule and the paddle, the rod will impulse a torque to the ratchet. Since the pawl prefers the ratchet to rotate in one direction, after a long run, the net rotation of the ratchet will be observed in the expected direction. The rotation of a ratchet can be used to do work. Although the expected work extracted from this device should be very small, it extracted the thermal energy of the bath and did useful work.

Feynman demonstrated that the ratchet should not work when $T_1=T_2$. The pawl has the same temperature as the environment. As a result, the pawl itself vibrates randomly and fails to operate as designed.

Subsequently, many researchers derived simplified models to test Feynman's proposal. Jarzynski and Mazonka [15] introduced a simple realization of Feynman's ratchet and pawl system, and indicated that their model can act both as a heat engine and as a refrigerator. However, there is no molecular-dynamics result to support their conclusion. Meurs and his co-workers [16] mentioned several models to show rectifications of thermal fluctuations, but only analytical results have been presented. Other attempts include (1) employing the overdamped Fokker-Planck equations with stochastic variables to simulate Feynman's ratchet and pawl [17] and (2) modeling asymmetric Brownian particles immersed in thermal baths [18,19]. The former one overly simplifies the gas-particle dynamics, and the latter one has no well-defined Maxwell's demon. Velasco and his co-workers [20] carefully considered the efficiency of the Feynman's ratchet, but the model is too simple to represent Feynman's system and there is no simulation result. Schneider and his co-workers [21] simulated Brownian motion of interacting particles which couples with a periodic potential and is driven by an external force. However, in their simulation, the Brownian particles are driven by Langevin force and their system is quite different from Feynman's setting.

*ghc@everest.hku.hk

Magnasco [22] considered a Brownian particle in a periodic potential under heavy damping, and obtained analytical results by using Fokker-Planck equation. He found that the Brownian particle cannot get any net drift speed, even if the symmetry of the potential is broken. Subjected to an external force with time correlations, the particle can exhibit a net drift speed. Magnasco and Stolovitzky [17] later presented an analytical result to test Feynman's ratchet and pawl system. However, in order to obtain analytical solution of Fokker-Planck equation, they concentrated on the overdamped region. Schneider and his co-workers [21] simulated a Brownian motion of noninteracting particles with an external force in a periodic potential. Risken and Voigtlaender solved the Fokker-Planck equation for the extremely underdamped Brownian motion in a double-well potential [23]. Astumian and Bier [24] also did similar analysis on heavily damped Brownian particle in a periodic potential and found that even the net force is zero a net flow can be induced by adding a fluctuation of the energy barrier. However, in their simulation, the potential applied to the Brownian particle is too simple to represent original Feynman's system.

In our previous work [3], we have introduced a simplified trap-door Maxwell's demon, and molecular-dynamics calculations were carried out to evaluate detailed behavior of such a system. Results show that no temperature differentiation is established when the trap door and the particles are in thermal equilibrium. When the trap door is coupled to low-temperature bath, as expected, the operation of the trap door leads to a temperature and a density gradient between the two chambers.

After dramatic improvement of nanotechnology, it is feasible to fabricate the structures with feature size less than 10 nm [25–28]. However, the construction of functional nanoelectromechanical systems (NEMSs) is hindered by the inability to provide power sources to NEMSs [29–36]. As we know, thermal fluctuation plays a very important role at nanometer scale. However, in most of existing designs for NEMSs, thermal fluctuation is usually neglected. The molecular-dynamics simulation of NEMSs provides useful information about the effects of thermal fluctuation at such scales. Since there is no realistic molecular-dynamics simulation on Feynman's ratchet and pawl system, we propose here two simplified Feynman's systems and perform the detailed molecular-dynamics and Langevin dynamics simulations to study their dynamics.

II. MODEL I

Model I contains two identical chambers which are filled with random distributed gas particles. Several pawls are placed in the upper chamber and the ratchet is consisted of a simple stick and another perpendicular joint stick. The angle of two sticks is fixed as shown in Fig. 1. The gas molecules are hard dishes moving in a two-dimensional space and can collide with each other. All collisions of gas molecules are energy and momentum conserving. After particle-wall collisions, the particle momentum reverses its component perpendicular to the wall. Geometrically, the pawl, the ratchet, and the perpendicular stick are line segments of zero width and impenetrable by the molecules (the mass of the perpendicular stick is zero). A spring with an angular force constant K_ϕ is fixed in one end of the pawl. In the equilibrium position, the pawl angle is ϕ_0.

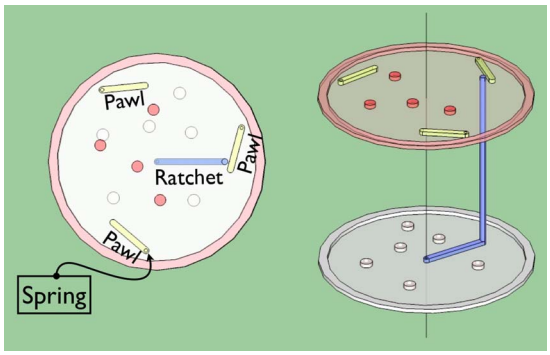

FIG. 1. (Color online) An illustration of the ratchet and pawl system. Left: top view. Right: side view. Both chambers are filled with gas particles, a spring is attached inside one end of each pawl, and the ratchet in lower chamber can rotate freely.

The ratchet is a free rotor. It changes its angular velocity upon collision. The change in the angular velocity is given in Appendix A. The Lagrangian of the pawl can be written as

$$L = \frac{1}{2}\sum_{i=1}^{N} m_{\text{gas}} v_i^2 + \frac{1}{2} I_{\text{pawl}} \dot{\phi}^2 - \frac{1}{2} K_\phi (\phi - \phi_0)^2 - V_{\text{int}}, \quad (1)$$

where v_i is the velocity of the ith gas particle; ϕ (ϕ_0) is the pawl angle (equilibrium pawl angle); $\dot{\phi}$ is the angular velocity; K_ϕ is the elastic constant of the pawl spring; m_{gas} and I_{pawl} are the mass of the gaseous particles and the momentum of inertia of the pawl, respectively; and V_{int} is the interaction potential energy among all rigid bodies in the system, which is constant except when particle-pawl and ratchet-pawl collisions occur. The third term on the right-hand side of equation describes the interaction between the spring and the pawl. Equations of motion for the particle velocities and the pawl angle ϕ are then derived from the Lagrangian. For instance, in the absence of collisions, the pawl angle $\phi(t)$ follows

$$\phi(t) = \phi_0 + [\phi(t_i) - \phi_0]\cos\left[\sqrt{\frac{K_\phi}{I_{\text{pawl}}}}(t - t_i)\right] + \dot{\phi}(t_i)\sqrt{\frac{I_{\text{pawl}}}{K_\phi}}\sin\left[\sqrt{\frac{K_\phi}{I_{\text{pawl}}}}(t - t_i)\right], \quad (2)$$

where $t \geq t_i$, where t_i denotes the starting time.

A. Molecular-dynamics simulation

A FORTRAN code is written for the molecular-dynamics simulation. Figure 2 is the flowchart of the program. The whole program consists of four major subroutines (read parameters, initialization, main loop, and finalization). "Read parameter" is for reading the simulation conditions and initial parameters. "Initialization" is for initializing the gas particles with Maxwell's distributed velocities. "Finalization" is

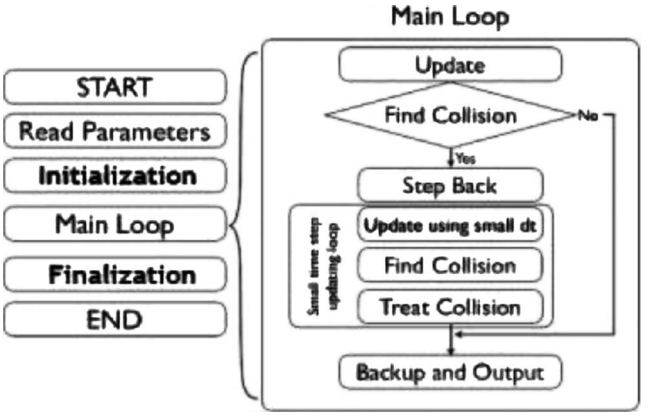

FIG. 2. Flowchart of the program. Left: structure of main program. Right: detailed structure of main loop procedure.

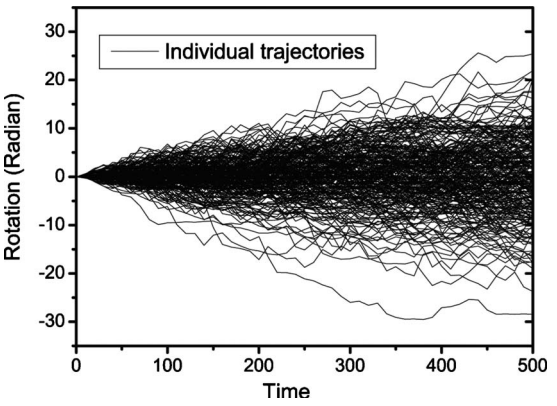

FIG. 3. 1000 individual simulation trajectories for model I.

used for saving simulation parameters in order to resume interrupted calculations. The detail of main loop is shown in the right part of Fig. 2. After entering the main loop, the forces, accelerations, velocities, and coordinates are updated with a given time step. Then, by comparing with the last step, a subroutine called "find collision" is called to search colliding events occurred in the current step. If there are collisions, all updated information is restored to previous step and the program enters the "small time step updating loop." In this loop (right middle part of Fig. 2), first, the program updates all valuables with smaller time step; the find collision subroutine is called and it records all collisions happened in this step. Finally, the "treat collision" subroutine is called to treat all recorded colliding events. After the small time step updating loop, the program will go back to the main loop and update the coordinates and velocities with original time steps.

In the simulation, a set of parameters is chosen as follows: the number of particles in each chamber $N=8$, the number of pawls $N_P=6$, the radius of each chamber $R=3.5$, the equilibrium pawl angle $\phi_0=46°$, the mass of the gas molecules in lower chamber $m_{\text{gas1}}=20$, the mass of the gas molecules in upper chamber $m_{\text{gas2}}=m_{\text{gas1}}\sqrt{T_2/T_1}$ (mass of particle in pawl chamber should be scaled down to have similar velocities as particles in ratchet chamber), the length of the ratchet $R_B=2.0$, the length of the pawl $R_L=0.8$, the mass of the ratchet $m_B=20$, the mass of the pawl $m_L=10$, the distance between the fixed point of pawl and the center of chamber $R_P=2.4$, the temperature of ratchet chamber $T_1=1000$, and the force constant $K_\phi=3500$. Our simulation takes typically several hours using a standard Pentium 4 processor. The compounded numerical error in the total energy of the system is kept below 10^{-10}.

The initial positions of gas molecules are randomly given, and their velocities are initialized according to the Boltzmann distribution as discussed in our previous work. The "velocity Verlet" algorithm is used in these simulations. The time evolution of the system is simulated by adopting the following algorithm: to minimize numerical errors, adaptable time steps are used. There are two kinds of time steps. Our program iterates a main cycle which starts from t_0 to the end of simulation with a time step $\Delta t=0.0001$. Within each cycle, the velocities and positions of all particles, the ratchet, and the pawls are updated assuming there is no collision. After the update of this time step, a subroutine is called to examine the colliding events. Four types of collision events are considered: particle-particle, particle-wall, particle-ratchet, and particle-pawl collisions. Information of the previous step is recorded to make a restoration. The criteria are (1) particle-particle collision: the distance between two particles is less than the diameter of a particle; (2) particle-ratchet collision (particle-pawl collisions are the same): the distance between particle and ratchet is less than the radius of a particle; (3) ratchet-pawl collision: the rotating end of ratchet cross the pawl.

Take a particle-particle collision as an example. At the end of each time step, the center-of-mass distance between two particles is measured to determine whether they collide. If there is no collision, the simulation is carried on to the next time step. Otherwise, the simulation is restored to previous state, and the time step is reduced to $\Delta t'=10^{-3}\Delta t$. After the restoration, the program performs 10^3 steps using $\Delta t'$. One regular step is divided into 10^3 small steps when collisions occur. After the collision, the simulation returns to the main loop with the original time step Δt. If a three-body collision is to occur, our program will record all the relevant information and stops. However, such a three-body collision event has not been encountered in our system which is composed of 16 particles with a time step $\Delta t'$ as small as $10^{-3}\Delta t$. Details on all collision events are handled and explained in Appendix A. For a particle-wall collision, the normal component of the particle's velocity reverses its direction while the tangential counterpart remains unchanged.

We set no temperature difference between the ratchet and the pawl chambers. Figure 3 shows 1000 individual runs of this model. In these trajectories, some of them rotate clockwise while others rotate counterclockwise. In an individual trajectory, we observe two ratchet-pawl collision events. First, the rotor gets enough energy from hot particles and crosses the barrier of bending potential of the angle ϕ. Second, the vibrating pawl hits the rotor and then the rotor bounces back.

Figure 4 shows the averaged results. The solid line is the net rotation of the rotor averaging the 1000 trajectories, and the dashed line represents their standard deviation. After averaged over 1000 individual trajectories, the net rotation of

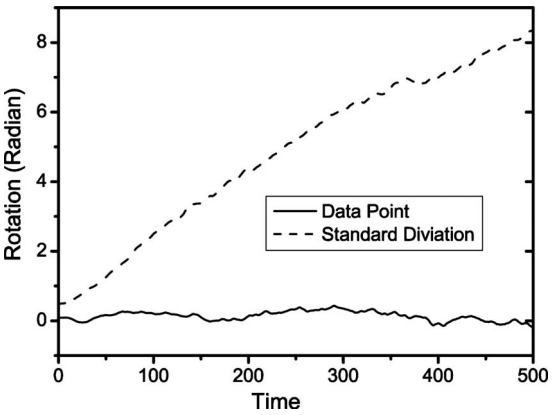

FIG. 4. Averaged rotation of the ratchet in one chamber system.

the ratchet is zero when applying lower temperature to pawl's chamber (T_2). As expected, the averaged result of the rotor rotates clockwise as shown in Fig. 5. The temperatures of two chambers are controlled by resetting the overall kinetic energies of their gaseous particles. Considering individual trajectory of this case, there are also two visual processes as we discussed. After applying lower temperature to the pawl's chamber, the vibrations of the pawl are greatly depressed by colliding with cool particles. Therefore, the first process becomes dominant, and the ratchet rotates as designed.

After fitting with a straight line, we calculate the angular velocity of the ratchet. Figure 5 shows three different results of the ratchet with different T_1/T_2. The angular velocity becomes larger when bigger temperature difference is applied.

After testing several combinations of T_1/T_2 while T_1 is set to 10^3, as shown in Fig. 6, when T_1/T_2 goes to 1, the ratchet has no net rotation. Angular velocities of the ratchet increased when T_1/T_2 became larger. When T_1/T_2 is larger than 10^3, the temperature of the pawl, T_2, is less than 1, it is low enough to suppress its fluctuation, and the angular velocity of the ratchet reaches its saturation value, which is determined by the average frequency that the ratchet hits the pawls.

To test the efficiency of the ratchet, temperature difference $T_1/T_2=10^3$ is used in the relevant simulations. We apply a constant torque to the ratchet against the desired rotating direction. The heat flow from the ratchet chamber to pawl chamber is calculated by summarizing the energy change of ratchet (or pawl) on each ratchet-pawl collision.

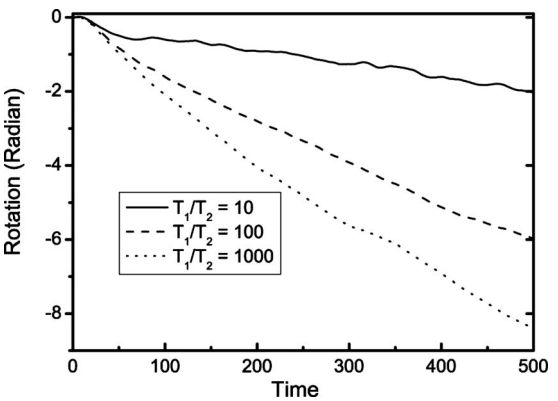

FIG. 5. Rotation of ratchet with different temperature configurations.

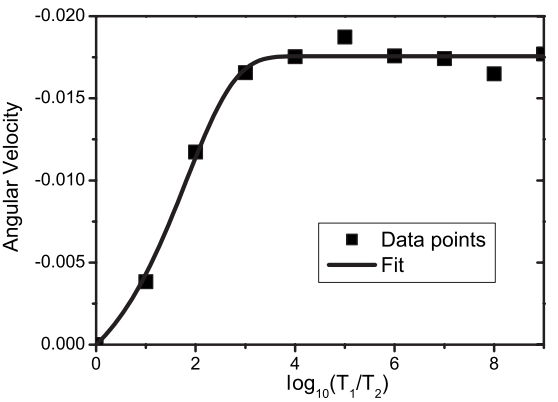

FIG. 6. Angular velocity of ratchet with different temperature configurations.

Figure 7 shows the efficiency of the system when different torques are applied. The result shows that the maximum efficiency is 0.262% when the torque is equal to 1.5×10^{-4}. When the torque exceeds 3.1×10^{-4}, the rotor rotates to the opposite direction; hence, the efficiency becomes negative.

The number of particles included in each chamber is considered. Figure 8 shows that the angular velocity of the ratchet decreases when a large number of gas particles are used. It is because that the rotation will be heavily blocked by gas particles when density of particles is too high.

After introducing and simulating this simplified ratchet and pawl system, a clear picture of such a system is shown. When there is no temperature difference between the ratchet chamber and the pawl chamber, no net rotation will be observed. After lowering the temperature to the pawl chamber, the fluctuations of the pawls are greatly depressed, and hence the ratchet rotates as designed. Different simulation temperatures are used, and we found that higher temperature difference results in higher rotation speed for $T_1/T_2<10^3$, and the average angular velocity saturates for $T_1/T_2>10^3$. The efficiency of the system has also been examined. The maximum efficiency is 0.262% when the external torque is equal to

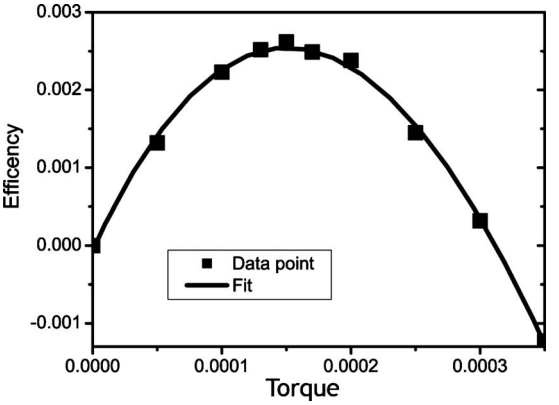

FIG. 7. Efficiency of the ratchet and pawl system when applying different torques.

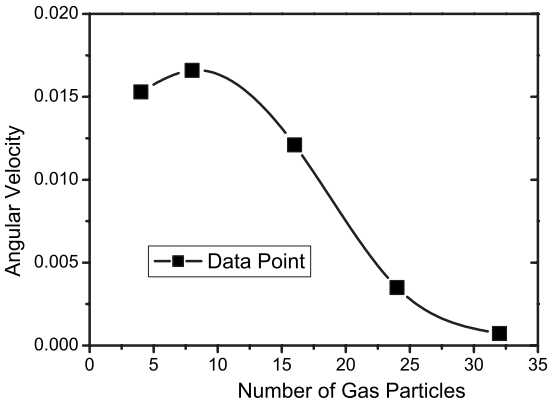

FIG. 8. Effect of different numbers of gas particles.

1.5×10^{-4}. This is much lower than the efficiency of the corresponding Carnot cycle, and thus implies that the net change of the total entropy is positive. External torque exceeding 3.1×10^{-4} results in counterclockwise rotation of the ratchet as the effect of the external force dominates over the rectification effect of the ratchet.

B. Langevin dynamics simulation

Langevin equation is commonly used to simulate the Brownian motion of systems subjected to fluctuation. It is a stochastic differential equation. A form of the Langevin equation for Brownian motion is as follows:

$$\frac{dv}{dt} = -\gamma v + F(x) + \Gamma(t), \tag{3}$$

where v is velocity, x is position, $F(x)$ is the force acted on the particle, and Γ is a Langevin force which is a stochastic form and satisfies $\langle\Gamma(t)\rangle=0$ and $\langle\Gamma(t)|\Gamma(t')\rangle=q\delta(t-t')$ (q is correlation constant). To solve this equation, one way is to count many individual trajectories or introduce a distribution density function and solve the related Fokker-Planck equation.

Figure 9 is an illustration of the simplified model of Feynman's ratchet and pawl system. The ratchet and pawl are both nonpenetrable straight sticks with zero width and certain mass, m_θ and m_ϕ. The ratchet can rotate freely around the center as well as the pawl can rotate around the fixed point with a spring attached on the point. The equilibrium position of the pawl is ϕ_0. There are Gaussian-type random forces on both the ratchet and the pawl.

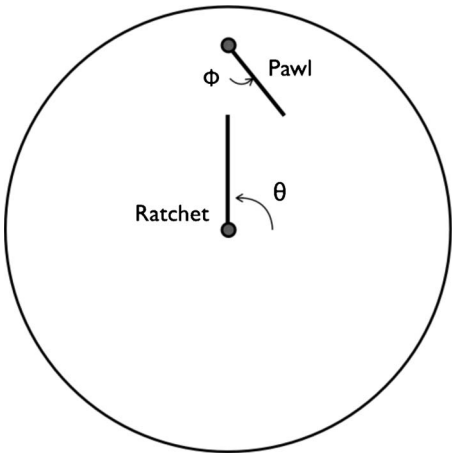

FIG. 9. An illustration of the simplified Feynman's ratchet and pawl system for Fokker-Planck equation.

The related Langevin equation can be written as

$$\dot{\omega}_\theta = -\gamma\omega_\theta - f_\theta(\theta,\phi,\dot{\theta},\dot{\phi}) + \Gamma_\theta(t),$$

$$\dot{\theta} = \omega_\theta,$$

$$\dot{\omega}_\phi = -\gamma\omega_\phi - f_\phi(\theta,\phi,\dot{\theta},\dot{\phi}) + \Gamma_\phi(t),$$

$$\dot{\phi} = \omega_\phi. \tag{4}$$

Here, the random forces acted on θ and ϕ are uncorrelated and both are distributed in Gaussian type; we have

$$\langle\Gamma_\theta(t)\Gamma_\theta(t')\rangle = \frac{2\gamma_\theta kT_\theta}{I_\theta}\delta(t-t'),$$

$$\langle\Gamma_\phi(t)\Gamma_\phi(t')\rangle = \frac{2\gamma_\phi kT_\phi}{I_\phi}\delta(t-t'),$$

$$\langle\Gamma_\theta(t)\Gamma_\phi(t')\rangle = 0, \tag{5}$$

where k is the Boltzmann constant, T_θ and T_ϕ are the temperatures of the ratchet and the pawl, γ_θ and γ_ϕ are friction coefficients, and I_θ and I_ϕ are the momentum inertia of the ratchet and the pawl, respectively.

The related Fokker-Planck equation can be written as follows [37]:

$$\frac{\partial}{\partial t}W(\theta,\phi,\dot{\theta},\dot{\phi},t) = \left\{-\frac{\partial}{\partial\theta}\dot{\theta} + \frac{\partial}{\partial\dot{\theta}}(f_\theta+\gamma_\theta\dot{\theta}) + \gamma_\theta\frac{kT}{I_\theta}\frac{\partial^2}{\partial\dot{\theta}^2} - \frac{\partial}{\partial\phi}\dot{\phi} + \frac{\partial}{\partial\dot{\phi}}(f_\phi+\gamma_\phi\dot{\phi}) + \gamma_\phi\frac{kT}{I_\theta}\frac{\partial^2}{\partial\dot{\theta}^2}\right\}W(\theta,\phi,\dot{\theta},\dot{\phi},t). \tag{6}$$

Here, $f_\theta=f_\theta(\theta,\phi,\dot{\theta},\dot{\phi})$ and $f_\phi=f_\phi(\theta,\phi,\dot{\theta},\dot{\phi})$ are forces acted on ratchet and pawl. There are abrupt changes in these functions when the ratchet collides to the pawl. [Here, $f_\theta=\delta\dot{\theta}I_\theta$ and $f_\phi=\delta\dot{\phi}I_\phi-k_\phi(\phi-\phi_0)$.] Detailed definitions of $\delta\dot{\theta}$ and $\delta\dot{\phi}$ are in Appendix A. Equation (6) is a four-variable time-dependent Fokker-Planck equation. There is no analytical solution [37]. To numerically solve the equation and determine the distribution function, one way is to use finite grid space, guess an initial distribution density function, and solve it by iteration. However, for a four-variable Fokker-Planck equation, it is very time consuming. The easiest way is to statistically solve the related Langevin equation [37] (calculate a large number of individual trajectories) and calculate the distribution function of the system.

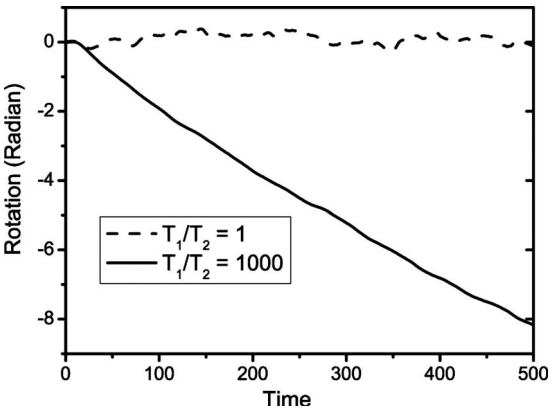

FIG. 10. Net rotation in different T_1 and T_2.

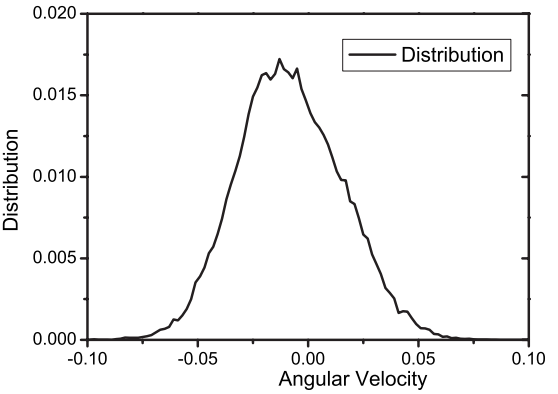

FIG. 11. Distribution of $\dot{\theta}$.

The setting in this simulation is very similar to the molecular-dynamics simulation. The major difference is that the particles in chambers are replaced with Langevin force. Compare to the molecular-dynamics simulation, the correlation between the environment and the ratchet (or the pawl) is much higher. The Langevin force continuously acts on the ratchet (or the pawl), while in previous case the gas particles only collide on the ratchet (or the pawl) occasionally. Therefore, the masses of the ratchet and the pawls are tuned to smaller values in order to have the similar angular velocities. In our case, the masses of the ratchet and the pawls are 100 times smaller.

In this simulation, to achieve similar results, a set of parameters is chosen as follows: the number of pawls $N_P=6$, the radius of each chamber $R=3.5$, the equilibrium ratchet angle $\phi_0=46°$, $R_B=2.0$, the length of the pawl $R_L=0.8$, the mass of the ratchet $m_B=0.2$, the mass of the pawl $m_L=0.1$, the temperature of ratchet chamber $T_1=10^9$, the distance between the fixed point of pawl and the center of chamber $R_P=2.4$, the force constant $K_\phi=3500$, and the friction constants of the ratchet and the pawl $\gamma_\theta=0.5$, $\gamma_\phi=5$. In order to have comparable results, the integration time step and total simulation time are set as $dt=0.0001$ and 500. Another FORTRAN code is written to perform this simulation. There are only ratchet-pawl collisions. The structure of the program is similar to the previous one. The Langevin force is applied to the system on all time steps. 1000 individual trajectories are counted to determine averaged values.

We test the condition with no temperature difference $T_1/T_2=1$. The result shows no difference as in molecular-dynamics simulations, as the dashed line in Fig. 10. No net rotation is observed. When the temperature of the two chamber is set to $T_1/T_2 \neq 1$, the rectifying effect occurs; the solid line in Fig. 10 shows that there is a net rotation when $T_1/T_2=1000$.

To observe the distribution density function of the system, we calculated the distribution of angular velocity of the ratchet ($\dot{\theta}$). Figure 11 is the distribution of $\dot{\theta}$. As it shows, the central point of the distribution is in -0.02, the average angular velocity of ratchet is negative, and the ratchet rotates to one direction as expected.

Different lengths of ratchet (other parameters are fixed) are adopted in the simulations. Figure 12 shows the relationship between the length of the ratchet and its average angular velocity. As all collisions are rigid body collisions, the rotation of the ratchet is thus mostly blocked by the pawl. Hence, the angular velocity is approximately zero when the ratchet length exceeds 2.2. Intuitively, there should be no rectifying effect when the ratchet cannot reach the pawl of equilibrium position. That means, in our configuration of the device, the length of ratchet should be larger than 1.843 in order to collide with the pawl. However, we found out that even though the ratchet is shorter than 1.843, a net rotation occurs. Figure 12 shows the angular velocity calculated in different lengths of ratchet. It is clear that the ratchet rotates to desired direction when the length is longer than 1.75. The reason is that the pawls are vibrating during the simulation, and there is a distribution of its angle. Figure 13 is the distribution of the pawl. It shows that the pawls have visible distribution in $52° > \phi > 40°$. This result shows that it has still the rectifying effect even when the length of ratchet is shorter than expected. When the length of the ratchet is shorter than 1.7, the ratchet cannot collide with the pawls at any angles, and the system has no rectifying effect and there is no net rotation. We calculated the efficiencies of our device with all the above configurations and found that their values are all much lower than that of the corresponding Carnot cycle. This implies that the net changes of total entropy are positive in all these cases.

The relation between angular velocity and different T_1/T_2 is also examined. Results are shown in Fig. 14. It is similar

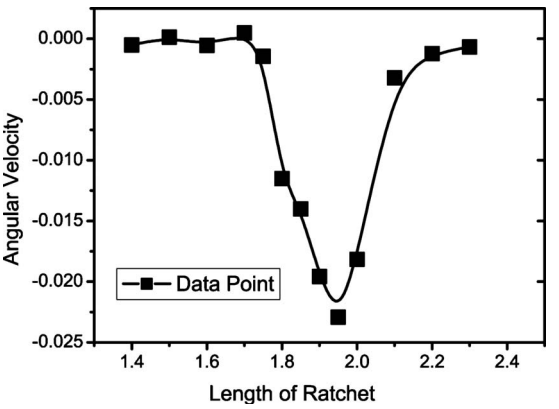

FIG. 12. Angular velocity with different lengths of ratchet.

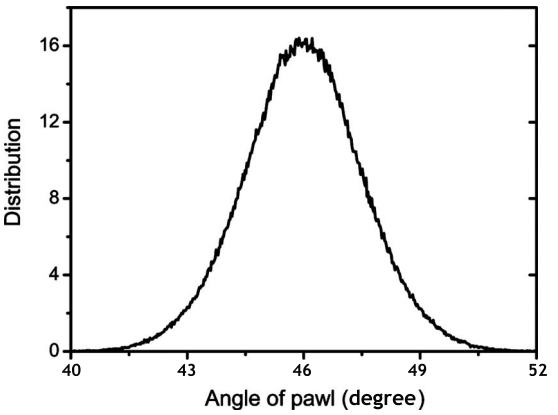

FIG. 13. Angle distribution of the pawl.

to the case of molecular-dynamics simulation. When the temperature difference is larger than $T_1/T_2=10^3$, the angular velocity saturates.

Different values of the friction coefficients of ratchet (γ_θ) are examined. Result is shown in Fig. 15. The angular velocity increases when friction coefficient becomes larger. However, when the friction coefficient is larger than 2.0, the curve becomes flat. Friction coefficient (γ_θ) is a physical parameter which measures the correlation between the object and the environment. The larger is the γ_θ, the larger are the Langevin force and the friction. As shown in the Langevin equation, the Langevin force is proportional to the square root of γ_θ and the friction force is proportional to γ_θ. Therefore, in the low damping region (lower γ_θ region), Langevin force is dominant. The angular velocity of the ratchet increases as γ_θ increases. However, in large γ_θ region (overdamping region), both Langevin force and friction are significant. Langevin force is canceled by friction. Hence, the curve became flat. The efficiency of this system is also tested for comparison. Result is shown in Fig. 16. There is a peak efficiency (0.152%) when the torque is equal to 5.5×10^{-4}.

Although the Fokker-Planck equation of the ratchet and pawl system is derived, we solve the problem by statistically counting a large number of individual trajectories of Langevin equation because there is no analytical solution. We obtain the similar results for molecular and Langevin dynamics by rescaling the temperatures and masses. After testing different configurations of parameters, we find that the ratchet rotates even when the length of ratchet is shorter than expected, and it is because the angle of pawl is distributed in a certain range. Different friction coefficients are also tested. In low damping region, larger friction coefficient results in larger angular velocity, and in large damping region friction coefficient can only slightly affect the angular velocity of the ratchet. The efficiency of this Langevin-force-driven system has been tested. The result is similar to the molecular-dynamics simulation. There is peak efficiency (0.152%) when the torque is equal to 5.5×10^{-4}.

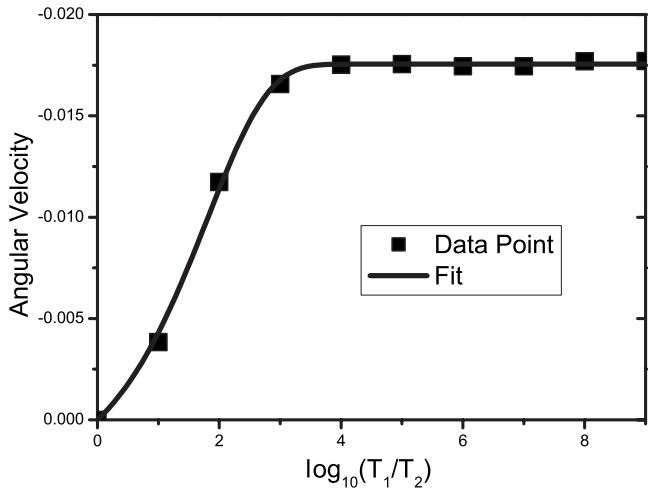

FIG. 14. Angular velocity in different temperature differences.

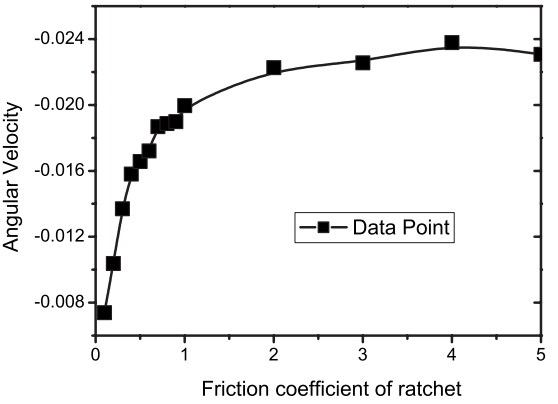

FIG. 15. Angular velocity and different friction coefficients.

III. MODEL II

There are many different designs of ratchet and pawl systems. In order to compare properties of different designs, in this section, we introduce a different design for Feynman's ratchet and pawl system as shown in Fig. 17. The system contains two identical circular chambers, placed with several pawls and a ratchet. The gas molecules are hard dishes moving inside a two-dimensional space and colliding with each other. All collisions of gas molecules are energy and momentum conserving. After particle-wall collisions, the particle momentum reverses its component perpendicular to the wall.

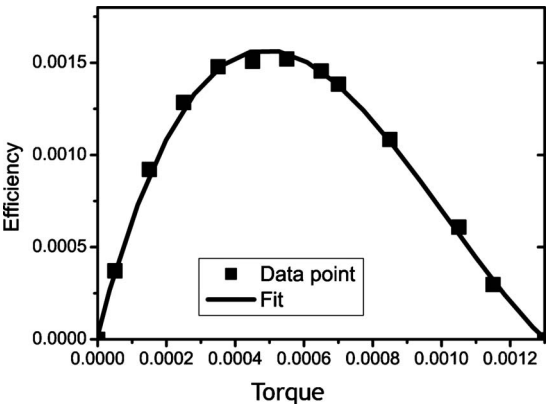

FIG. 16. Efficiency when applying external torque.

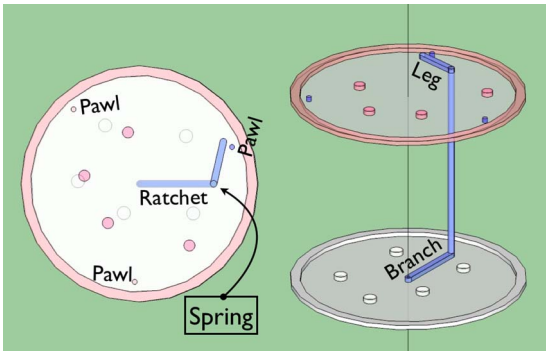

FIG. 17. (Color online) An illustration of the ratchet and pawl system. Left: top view. Right: side view.

The rotor consists of a branch, a leg, and a rod. The branch and the leg are connected by the perpendicular rod. Geometrically, the branch, the leg, and the rod are impenetrable line segments of zero width, and the rod between these two chambers is of zero mass. A spring with a force constant K_ϕ is placed in the rod between the branch and the leg. In the equilibrium state, the branch-leg angle is ϕ_0 as shown in Fig. 18.

The potential energy of the ratchet is

$$\mathrm{PE(ratchet)} = \tfrac{1}{2}K_\phi(\phi - \phi_e)^2. \tag{7}$$

The equations of motion (EOMs) for θ and ϕ are

$$\ddot{\theta} = \frac{m_L R_L R_B}{I_\theta}\left[\sin\phi\dot{\phi}\dot{\theta} + \frac{\sin\phi}{2}\dot{\phi}^2 + \frac{I_2\sin\phi}{2I_L}\dot{\theta}^2 + \frac{\cos\phi K_\phi}{2I_L}(\phi - \phi_0)\right] + \frac{K_\phi}{I_\theta}(\phi - \phi_0), \tag{8}$$

$$\ddot{\phi} = -\frac{m_L R_L R_B \sin\phi}{2I_L I_\theta}(I_1\dot{\theta}^2 + I_2\dot{\phi}^2 + 2I_2\dot{\phi}\dot{\theta}) - \frac{I_1}{I_L I_\theta}K_\phi(\phi - \phi_0). \tag{9}$$

Here, the moments of inertia are

$$I_B = \frac{1}{3}m_B R_B^2,$$

$$I_L = \frac{1}{3}m_L R_L^2,$$

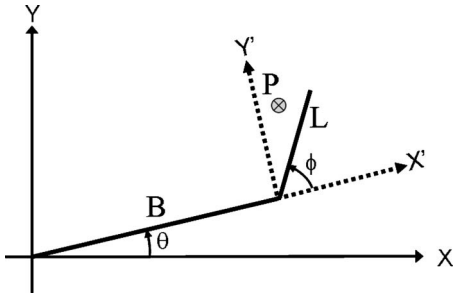

FIG. 18. Schematic representation of the ratchet and the pawl.

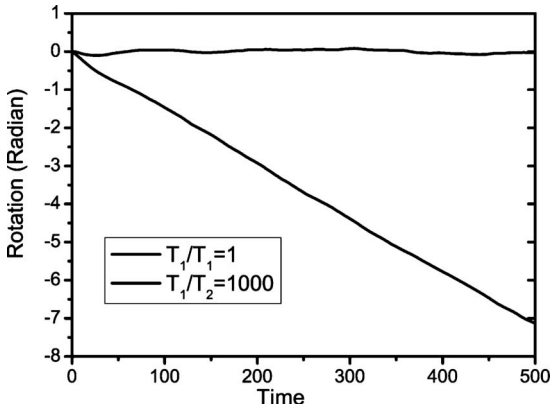

FIG. 19. Rotation of ratchet on different temperatures applied.

$$I_1 = I_B + I_L + m_L R_B^2 + m_L R_L R_B \cos\phi,$$

$$I_2 = I_L + \frac{1}{2}m_L R_L R_B \cos\phi,$$

$$I_\theta = \frac{I_1 I_L - I_2^2}{I_L}. \tag{10}$$

The detailed derivation is shown in Appendix B.

In the simulation, a set of parameters is chosen as follows: the number of particles in each chamber $N=8$, the radius of each chamber $r=3.5$, the equilibrium branch-leg angle $\phi_0 = 46°$, the length of the branch $R_B=2.0$, the length of the leg $R_L=0.8$, the length between the pawl and center point $R_P = 2.6$, the mass of the branch $m_B=20$, the mass of the leg $m_L=30$, the mass of gas particle in branch chamber $m_{\mathrm{gas1}} = 50$, the mass of gas particle in leg chamber $m_{\mathrm{gas2}} = m_{\mathrm{gas1}}\sqrt{T_2/T_1}$ (mass of particle in leg chamber should be scaled down to have similar velocities as particles in branch chamber), the size of gas particle $r_{\mathrm{gas}}=0.1$, time step $dt = 0.0001$, temperature of branch chamber $T_1=1000$, and the force constant $K_\phi=3500$. Collision events include particle-particle, particle-branch, particle-leg, and leg-pawl collisions. All special cases of collisions are considered (special cases are the gas particles that collide with the joint point of the branch and the leg, or with the tail of the leg).

As our previous results, the ratchet has no net rotation for $T_1=T_2$, as shown in Fig. 19. When $T_1/T_2=1000$, the ratchet rotates clockwise as expected.

Different temperatures are used. As shown in Fig. 20, it is similar to model I. When $T_1/T_2 > 1000$, the ratchet rotates at the similar speed even as T_2 is further lowered.

After applying different torques to the ratchet, as shown in Fig. 21, there is a maximum efficiency (1.12×10^{-5}) when the torque equals 0.0008. This maximum efficiency is much lower than that of model I.

The related Langevin equation can be written as

$$\dot{\omega}_\theta = -\gamma\omega_\theta - f_\theta(\theta,\phi,\dot{\theta},\dot{\phi}) + \Gamma_\theta(t),$$

$$\dot{\theta} = \omega_\theta,$$

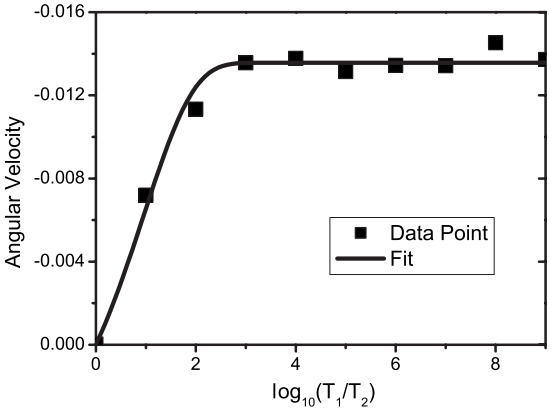

FIG. 20. Angular velocities on different temperature configurations.

$$\dot{\omega}_\phi = -\gamma\omega_\phi - f_\phi(\theta,\phi,\dot{\theta},\dot{\phi}) + \Gamma_\phi(t),$$

$$\dot{\phi} = \omega_\phi, \tag{11}$$

where the random forces acted on θ and ϕ. Here, $f_\theta = f_\theta(\theta,\phi,\dot{\theta},\dot{\phi})$ and $f_\phi = f_\phi(\theta,\phi,\dot{\theta},\dot{\phi})$ are interacting forces between branch and leg. Detailed equations of these forces (with collision and without collision) are in Appendix B. The parameters used to do this simulation are similar to those of the molecular-dynamics simulation except that the masses of the branch and the leg are set as $m_B=0.2$, $m_L=0.3$; the temperature of the branch is set to $T_1=10^7$; and the friction coefficients of the branch and the leg are set to 0.5 and 5.

The ratchet has no net rotation when applying same temperature to the branch and the leg, as well as it rotates clockwise when lower temperature is applied to the leg. As shown in Fig. 22. When $T_1/T_2=1000$, the ratchet rotates to the desired direction.

Different temperatures are used. As shown in Fig. 23, it has similar behaviors as the previous case. When $T_1/T_2 > 1000$, the ratchet rotates clockwise at the similar speed. After applying different torques to the ratchet, as shown in Fig. 24, when the torque is equal to 4×10^{-4}, there is a maximum efficiency (1.79×10^{-5}) (Fig. 25).

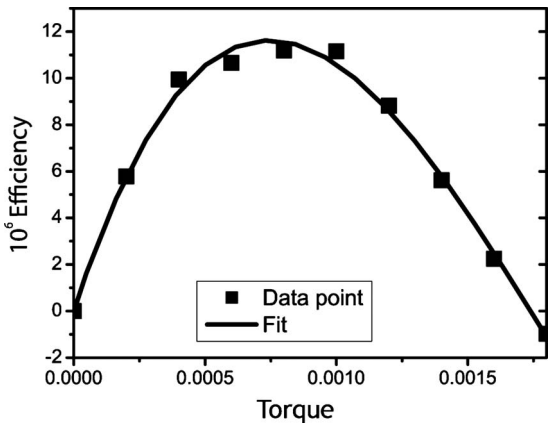

FIG. 21. Efficiency of ratchet when applying different torques.

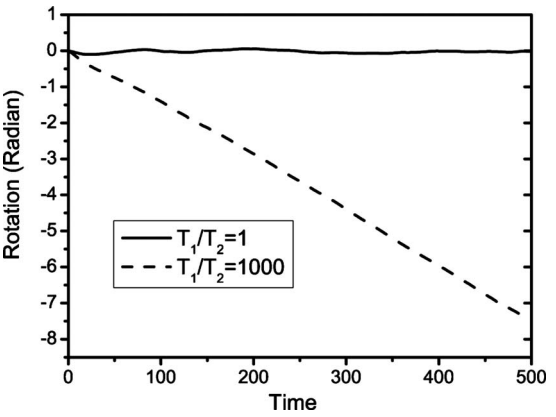

FIG. 22. Rotation of ratchet on different temperatures applied.

IV. SUMMARY AND DISCUSSION

In this work, we propose two designs for Feynman's ratchet and pawl system, and we have performed both molecular-dynamics and Langevin dynamics simulations for two designs to examine their detailed behavior. We find out that the ratchet rotates as designed when the temperature of the pawl chamber is lower than that of the ratchet. Several parameters and configurations have been tested. The results show that the ratchet's efficiency depends on the applied torque. After comparing results for different designs of ratchet, we find out that the efficiency of the ratchet depends greatly on the design. That may help us to design new nanodevices in the future.

ACKNOWLEDGMENTS

This work was supported by the Hong Kong Research Grants Council (Grants No. HKU 7012/04P, No. HKU 7127/05E, No. HKU 7011/06P, No. HKU 7013/07P, and No. N_HKU 764/05) and the Committee on Research and Con-

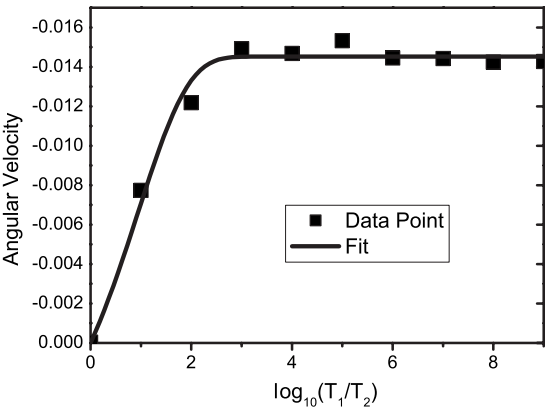

FIG. 23. Angular velocities on different temperature configurations.

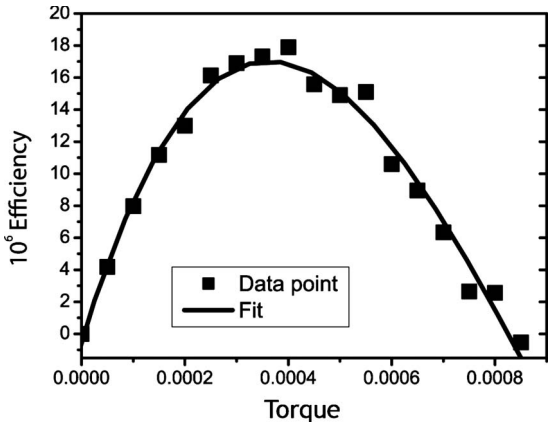

FIG. 24. Efficiency of ratchet when applying different torques.

ference Grants (CRCG) of University of Hong Kong.

APPENDIX A: DETAILS OF COLLISIONS FOR FEYNMAN'S RATCHET AND PAWL SYSTEM

1. Without collision

The potential energy of the ratchet and pawl is due to the spring attached to the pawl (leg),

$$\mathrm{PE(RP)} = \tfrac{1}{2}K_\phi(\phi - \phi_e)^2, \tag{A1}$$

where ϕ_e stands for the minimum position of the above parabolic potential. The moments of inertia of the leg with respect to point P and of the branch with respect to point O are

$$I_L = \tfrac{1}{3}m_L R_L^2,$$

$$I_B = \tfrac{1}{3}m_B R_B^2, \tag{A2}$$

respectively, as shown in Fig. 25. The EOM for ϕ is as follows:

$$I_L\ddot{\phi} = -K_\phi(\phi - \phi_e). \tag{A3}$$

The exact solution for the EOM is

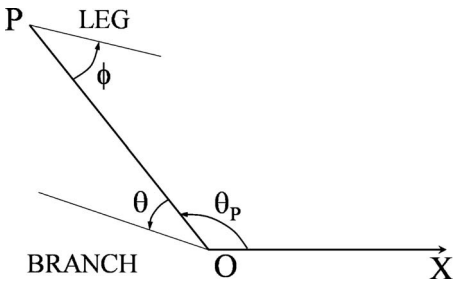

FIG. 25. For both θ and ϕ, the most convenient choice for range would be $(-\pi, \pi)$.

$$\phi(t) = \phi_e + [\phi(t_0) - \phi_e]\cos\left(\sqrt{\frac{K_\phi}{I_L}}t\right) + \dot{\phi}(t_0)\sqrt{\frac{I_L}{K_\phi}}\sin\left(\sqrt{\frac{K_\phi}{I_L}}t\right), \tag{A4}$$

where $\phi(t_0)$ and $\dot{\phi}(t_0)$ are the initial displacement and velocity for ϕ, respectively.

2. General formulation for collision events between particles and sticks

The change of velocities for the branch, the leg, and the gas molecules are denoted by $\delta\dot{\theta}$, $\delta\dot{\phi}$, and $\delta\dot{x}(\delta\dot{y})$, respectively. Upon a single collision event, they are determined via the following relations:

$$\delta\dot{\theta} = A\Delta P,$$

$$\delta\dot{\phi} = B\Delta P,$$

$$\delta\dot{x} = C\Delta P,$$

$$\delta\dot{y} = D\Delta P, \tag{A5}$$

where ΔP is

$$\Delta P = -2\frac{X}{Y},$$

$$X = AI_B\dot{\theta} + BI_L\dot{\phi} + Cm_G\dot{x} + Dm_G\dot{y},$$

$$Y = A^2I_B + B^2I_L + C^2m_G + D^2m_G,$$

$$A = \frac{\partial_\theta h}{I_B},$$

$$B = \frac{\partial_\phi h}{I_L},$$

$$C = \frac{\partial_x h}{m_G},$$

$$D = \frac{\partial_y h}{m_G}. \tag{A6}$$

Here, h represents the distance between the particle and the stick.

3. Ratchet hits pawl

$$h = R_P\sin\phi + R_B\sin(\theta - \phi),$$

$$\partial_\theta h = R_B\cos(\theta - \phi),$$

$$\partial_\phi h = R_P\cos\phi - R_B\cos(\theta - \phi),$$

$$C = 0,$$

$$D = 0. \tag{A7}$$

4. Gas hits ratchet

$$h = x \sin\theta - y \cos\theta,$$

$$\partial_\theta h = x \cos\theta + y \sin\theta,$$

$$\partial_x h = \sin\theta,$$

$$\partial_y h = -\cos\theta,$$

$$B = 0, \tag{A8}$$

where x and y are Cartesian coordinates in the system with $\overrightarrow{OP}$ as the positive x axis.

5. Gas hits the end of the ratchet

This happens when the gas molecule has a finite radius R,

$$h = \sqrt{(x - R_B \cos\theta)^2 + (y - R_B \sin\theta)^2} - R,$$

$$\partial_\theta h = \frac{R_B(x \sin\theta - y \cos\theta)}{R},$$

$$\partial_x h = \frac{x - R_B \cos\theta}{R},$$

$$\partial_y h = \frac{y - R_B \sin\theta}{R},$$

$$B = 0, \tag{A9}$$

where x and y are Cartesian coordinates in the system with $\overrightarrow{OP}$ as the positive x axis.

6. Gas hits leg

$$h = x \sin\phi - y \cos\phi,$$

$$\partial_\phi h = x \cos\phi + y \sin\phi,$$

$$\partial_x h = \sin\phi,$$

$$\partial_y h = -\cos\phi,$$

$$A = 0, \tag{A10}$$

where x and y are Cartesian coordinates in the system with $\overrightarrow{PO}$ as the positive x axis.

7. Gas hits the end of the pawl

This happens when the gas molecule has a finite radius R,

$$h = \sqrt{(x - R_L \cos\phi)^2 + (y - R_L \sin\phi)^2} - R,$$

$$\partial_\phi h = \frac{R_L(x \sin\phi - y \cos\phi)}{R},$$

$$\partial_x h = \frac{x - R_L \cos\phi}{R},$$

$$\partial_y h = \frac{y - R_L \sin\phi}{R},$$

$$A = 0, \tag{A11}$$

where x and y are Cartesian coordinates in the system with $\overrightarrow{PO}$ as the positive x axis.

8. Coordinate transformation

Assume that the geometric center of a gas molecule is at (x,y) in the $\overrightarrow{OX}$ coordinate system; its coordinates in $\overrightarrow{OP}$ and $\overrightarrow{PO}$ systems are (x_{OP}, y_{OP}) and (x_{PO}, y_{PO}), respectively. (x,y) can be transformed into (x_{OP}, y_{OP}) via

$$x_{OP} = x \cos\theta_P + y \sin\theta_P,$$

$$y_{OP} = y \cos\theta_P - x \sin\theta_P,$$

$$\dot{x}_{OP} = \dot{x} \cos\theta_P + \dot{y} \sin\theta_P,$$

$$\dot{y}_{OP} = \dot{y} \cos\theta_P - \dot{x} \sin\theta_P. \tag{A12}$$

(x,y) can be transformed into (x_{PO}, y_{PO}) via

$$x_{PO} = R_P - x \cos\theta_P - y \sin\theta_P,$$

$$y_{PO} = -y \cos\theta_P + x \sin\theta_P,$$

$$\dot{x}_{PO} = -\dot{x} \cos\theta_P - \dot{y} \sin\theta_P,$$

$$\dot{y}_{PO} = -\dot{y} \cos\theta_P + \dot{x} \sin\theta_P. \tag{A13}$$

APPENDIX B: DETAILS OF COLLISIONS FOR SECOND RATCHET AND PAWL SYSTEM

1. Coordinate transformation

Transformations between XY and $X'Y'$ coordinate systems are

$$x = x' \cos\theta - y' \sin\theta + R_B \cos\theta,$$

$$y = y' \cos\theta + x' \sin\theta + R_B \sin\theta,$$

$$x' = x \cos\theta + y \sin\theta - R_B,$$

$$y' = y \cos\theta - x \sin\theta. \tag{B1}$$

Velocity transformations between XY and $X'Y'$ coordinate systems are

$$v_x' = v_x \cos\theta + v_y \sin\theta - x \sin\theta\dot{\theta} + y \cos\theta\dot{\theta},$$

$$v_y' = -v_x \sin\theta + v_y \cos\theta - x \cos\theta\dot{\theta} - y \sin\theta\dot{\theta}. \quad \text{(B2)}$$

2. Without collision

The potential energy of the ratchet is

$$\text{PE(ratchet)} = \tfrac{1}{2}K_\phi(\phi - \phi_e)^2. \quad \text{(B3)}$$

Moments of inertia are

$$I_B = \tfrac{1}{3}m_B R_B^2,$$

$$I_L = \tfrac{1}{3}m_L R_L^2,$$

$$I_1 = I_B + I_L + m_L R_B^2 + m_L R_L R_B \cos\phi,$$

$$I_2 = I_L + \tfrac{1}{2}m_L R_L R_B \cos\phi,$$

$$I_\theta = \frac{I_1 I_L - I_2^2}{I_L}. \quad \text{(B4)}$$

EOMs for θ and ϕ are

$$\ddot{\theta} = \frac{m_L R_L R_B}{I_\theta}\left[\sin\phi\dot{\phi}\dot{\theta} + \frac{\sin\phi}{2}\dot{\phi}^2 + \frac{I_2 \sin\phi}{2I_L}\dot{\theta}^2 + \frac{\cos\phi K_\phi}{2I_L}(\phi - \phi_0)\right] + \frac{K_\phi}{I_\theta}(\phi - \phi_0), \quad \text{(B5)}$$

$$\ddot{\phi} = -\frac{m_L R_L R_B \sin\phi}{2I_L I_\theta}(I_1\dot{\theta}^2 + I_2\dot{\phi}^2 + 2I_2\dot{\phi}\dot{\theta}) - \frac{I_1}{I_L I_\theta}K_\phi(\phi - \phi_0). \quad \text{(B6)}$$

3. When a gas molecule hits the branch

Before collision the velocities are v_n, v_t, $\dot{\theta}$, and $\dot{\phi}$, respectively. After collision the velocities are $\tilde{v}_n$, $\tilde{v}_t$, $\tilde{\dot{\theta}}$, and $\tilde{\dot{\phi}}$, respectively. Define

$$R_G = \sqrt{x_G^2 + y_G^2},$$

$$v_G = \sqrt{v_n^2 + v_t^2},$$

$$C_\theta = -\frac{m_G R_G}{I_\theta} = \frac{m_G R_G I_L}{I_2^2 - I_1 I_L},$$

$$C_\phi = \frac{m_G I_2 R_G}{I_\theta I_L} = \frac{m_G R_G I_2}{I_1 I_L - I_2^2}. \quad \text{(B7)}$$

The change in velocity of the gas molecule perpendicular to the branch is

$$\delta v_n = \tilde{v}_n - v_n = \frac{-2I_\theta(v_n - R_G\dot{\theta})}{I_\theta + m_G R_G^2}. \quad \text{(B8)}$$

Therefore, the velocities after the collision are

$$\tilde{v}_n = \delta v_n + v_n,$$

$$\tilde{v}_t = v_t,$$

$$\tilde{\dot{\theta}} = C_\theta \delta v_n + \dot{\theta},$$

$$\tilde{\dot{\phi}} = C_\phi \delta v_n + \dot{\phi}. \quad \text{(B9)}$$

The transformation between v_n, v_t and v_x, v_y is

$$v_n = v_y \cos\theta - v_x \sin\theta,$$

$$v_t = v_y \sin\theta + v_x \cos\theta,$$

$$\tilde{v}_n = \tilde{v}_y \cos\theta - \tilde{v}_x \sin\theta,$$

$$\tilde{v}_t = \tilde{v}_y \sin\theta + \tilde{v}_x \cos\theta,$$

$$v_x = -v_n \sin\theta + v_t \cos\theta,$$

$$v_y = v_n \cos\theta + v_t \sin\theta,$$

$$\tilde{v}_x = -\tilde{v}_n \sin\theta + \tilde{v}_t \cos\theta,$$

$$\tilde{v}_y = \tilde{v}_n \cos\theta + \tilde{v}_t \sin\theta. \quad \text{(B10)}$$

4. When a gas molecule hits the leg

Before collision the velocities are v_x, v_y, $\dot{\theta}$, and $\dot{\phi}$, respectively. After collision the velocities are $\tilde{v}_x$, $\tilde{v}_y$, $\tilde{\dot{\theta}}$, and $\tilde{\dot{\phi}}$, respectively. Define

$$R_G' = \sqrt{x_G'^2 + y_G'^2},$$

$$D_{x\theta} = \frac{m_G R_B R_G' \cos\phi(2I_L - m_L R_L R_G')}{2I_L I_\theta(y_G - R_B \sin\theta)},$$

$$D_{x\phi} = \frac{m_G R_G'(I_1 R_G' - I_2 R_G' - I_2 R_B \cos\phi)}{I_L I_\theta(y_G - R_B \sin\theta)},$$

$$D_{xy} = -\frac{x_G - R_B \cos\theta}{y_G - R_B \sin\theta}. \quad \text{(B11)}$$

The change in velocity of the gas molecule along the x direction is

$$\delta v_x = \tilde{v}_x - v_x = \frac{-2m_G}{I_1 D_{x\theta}^2 + I_L D_{x\phi}^2 + 2I_2 D_{x\theta} D_{x\phi} + m_G D_{xy}^2 + m_G} v_x - 2\frac{I_1 D_{x\theta}\dot{\theta} + I_L D_{x\phi}\dot{\phi} + I_2 D_{x\theta}\dot{\phi} + I_2 D_{x\phi}\dot{\theta} + m_G D_{xy} v_y}{I_1 D_{x\theta}^2 + I_L D_{x\phi}^2 + 2I_2 D_{x\theta} D_{x\phi} + m_G D_{xy}^2 + m_G}. \quad \text{(B12)}$$

Therefore, the velocities after the collision are

$$\tilde{v}_x = \delta v_x + v_x,$$

$$\tilde{v}_y = D_{xy}\delta v_x + v_y,$$

$$\tilde{\dot{\theta}} = D_{x\theta}\delta v_x + \dot{\theta},$$

$$\tilde{\dot{\phi}} = D_{x\phi}\delta v_x + \dot{\phi}. \tag{B13}$$

5. When the leg hits the pawl

Since the pawl does not move, before and after the collision the velocities are $\dot{\theta}, \dot{\phi}$ and $\tilde{\dot{\theta}}, \tilde{\dot{\phi}}$, respectively. Define

$$D_{\theta\phi} = \frac{D_{x\phi}}{D_{x\theta}} = \frac{2I_2R_B\cos\phi - 2I_BR'_G - 2m_LR_B^2R'_G - m_LR_LR_BR'_G\cos\phi}{m_LR_LR_BR'_G\cos\phi - 2I_LR_B\cos\phi}. \tag{B14}$$

The velocities after the collision are

$$\tilde{\dot{\theta}} = \frac{(I_LD_{\theta\phi}^2 - I_1)\dot{\theta} - 2(I_LD_{\theta\phi} + I_2)\dot{\phi}}{I_1 + I_LD_{\theta\phi}^2 + 2I_2D_{\theta\phi}},$$

$$\tilde{\dot{\phi}} = \frac{(I_1 - I_LD_{\theta\phi}^2)\dot{\phi} - 2(I_1D_{\theta\phi} + I_2D_{\theta\phi}^2)\dot{\theta}}{I_1 + I_LD_{\theta\phi}^2 + 2I_2D_{\theta\phi}}. \tag{B15}$$

When $\phi = \frac{\pi}{2}$ or $\frac{3\pi}{2}$, $\cos\phi = 0$, the velocities after the collision are

$$\tilde{\dot{\theta}} = \dot{\theta},$$

$$\tilde{\dot{\phi}} = -\dot{\phi} - 2\dot{\theta}. \tag{B16}$$

[1] J. C. Maxwell, *Theory of Heat* (Appleton, London, 1871).
[2] W. Thomson, Nature (London) **9**, 441 (1874).
[3] J. Zheng, X. Zheng, Y. Zhao, Y. Xie, C. Y. Yam, G. H. Chen, Q. Jiang, and A. T. Chwang, Phys. Rev. E **75**, 041109 (2007).
[4] Y. Zhao, C. C. Ma, L. H. Wang, G. H. Chen, Z. P. Xu, Q. S. Zheng, Q. Jiang, and A. T. Chwang, Nanotechnology **17**, 1032 (2006).
[5] Y. Zhao, C. C. Ma, G. H. Chen, and Q. Jiang, Phys. Rev. Lett. **91**, 175504 (2003).
[6] C. C. Ma, Y. Zhao, C. Y. Yam, G. H. Chen, and Q. Jiang, Nanotechnology **16**, 1253 (2005).
[7] Y. Zhao, C. C. Ma, L. H. Wong, G. H. Chen, Z. P. Xu, Q. S. Zheng, Q. Jiang, and A. T. Chwang, J. Comput. Theor. Nanosci. **3**, 852 (2006).
[8] X. Wang, H. Xin, J. N. Leonard, G. H. Chen, A. T. Chwang, and Q. Jiang, J. Nanosci. Nanotechnol. **7**, 1512 (2007).
[9] Z. Xu, Q. S. Zheng, and G. H. Chen, Phys. Rev. B **75**, 195445 (2007).
[10] M. v. Smoluchowski, Phys. Z. **13**, 1069 (1912).
[11] K. Zhang and K. Zhang, Phys. Rev. A **46**, 4598 (1992).
[12] P. Skordos and W. Zurek, Am. J. Phys. **60**, 876 (1992).
[13] H. Leff and A. Rex, *Maxwell's Demon 2* (Institute of Physics, London, 2003).
[14] R. P. Feynman, R. B. Leighton, and M. Sands, *The Feynman Lectures on Physics I* (Addison-Wesley, Reading, MA, 1963), Chap. 46.
[15] C. Jarzynski and O. Mazonka, Phys. Rev. E **59**, 6448 (1999).
[16] P. Meurs, C. Van den Broeck, and A. Garcia, Phys. Rev. E **70**, 051109 (2004).
[17] M. O. Magnasco and G. Stolovitzky, J. Stat. Phys. **93**, 615 (1998).
[18] C. Van den Broeck, R. Kawai, and P. Meurs, Phys. Rev. Lett. **93**, 090601 (2004).
[19] C. Van den Broeck, P. Meurs, and R. Kawai, New J. Phys. **7**, 10 (2005).
[20] S. Velasco, J. M. M. Roco, A. Medina, and A. Calvo Hernandez, J. Phys. D: Appl. Phys. **34**, 1000 (2001).
[21] T. Schneider, E. P. Stoll, and R. Morf, Phys. Rev. B **18**, 1417 (1978).
[22] M. O. Magnasco, Phys. Rev. Lett. **71**, 1477 (1993).
[23] H. Risken and K. Voigtlaender, J. Stat. Phys. **41**, 825 (1985).
[24] R. D. Astumian and M. Bier, Phys. Rev. Lett. **72**, 1766 (1994).
[25] R. B. Marcus, T. S. Ravi, and T. Gmitter, Appl. Phys. Lett. **56**, 236 (1990).
[26] J. Sone *et al.*, Nanotechnology **10**, 135 (1999).
[27] D. W. Carr, L. Sekaric, and H. G. Craighead, J. Vac. Sci. Technol. B **16**, 3821 (1998).
[28] D. W. Carr, S. Evoy, L. Sekaric, J. M. Parpia, and H. G. Craighead, Appl. Phys. Lett. **75**, 920 (1999).
[29] C. D. Montemagno and G. D. Bachand, Nanotechnology **10**, 225 (1999).
[30] G. D. Bachand and C. D. Montemagno, Biomed. Microdevices **2**, 179 (2000).
[31] S. M. Block, Cell **93**, 5 (1998).
[32] M. J. Schnitzer and S. M. Block, Nature (London) **388**, 386 (1997).
[33] M. Wang *et al.*, Science **282**, 902 (1998).
[34] K. Kitamura, M. Tokunaga, A. H. Iwane, and T. Yanagida, Nature (London) **397**, 129 (1999).
[35] R. Yasuda, H. Noji, K. Kinosita, Jr., and M. Yoshida, Cell **93**, 1117 (1998).
[36] H. Noji, R. Yasuda, M. Yoshida, and K. Kinosita, Jr., Nature (London) **386**, 299 (1997).
[37] H. Risken, *The Fokker-Planck Equation* (Springer-Verlag, Berlin, 1989).